Seeing the Air: An Overview of Atmospheric Lidar

by
Dr. Leda Sox
Senior Research Scientist
Georgia Tech Research Institute

With
Dr. Christopher R. Valenta, GTRI
Dr. Gary G. Gimmestad, GTRI/GTPE

LIght Detection And Ranging (LIDAR)

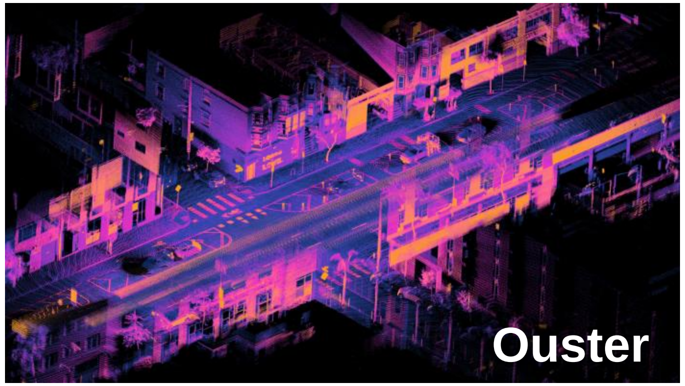

Lidar for Autonomous Vehicles

“Hard-target” Lidar

Ranging from: $R = ct/2$

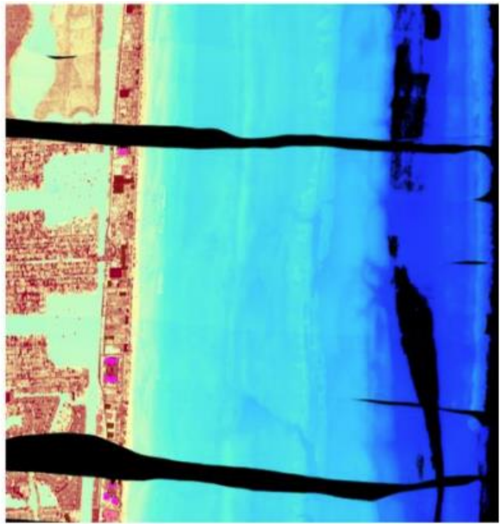

Bathymetric Lidar

Brown et al., 2019

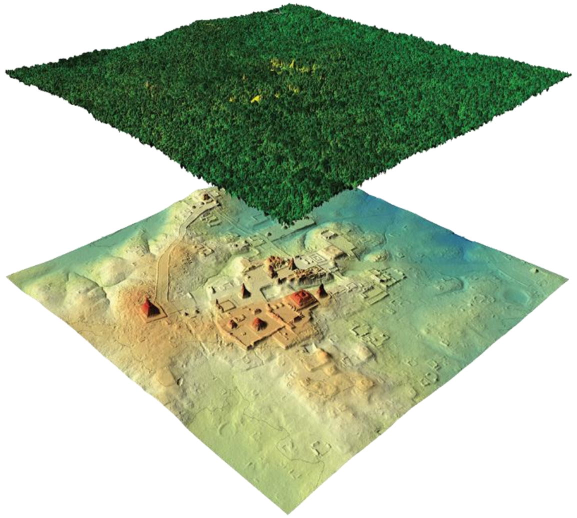

Topographic Lidar

Moller & Fernandez-Diaz, 2019

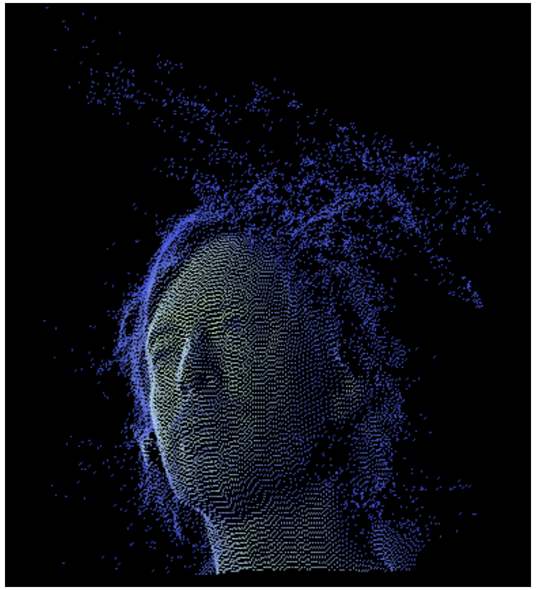

Radiohead’s House of Cards music video

Using Atmospheric Lidar to "See the Air"

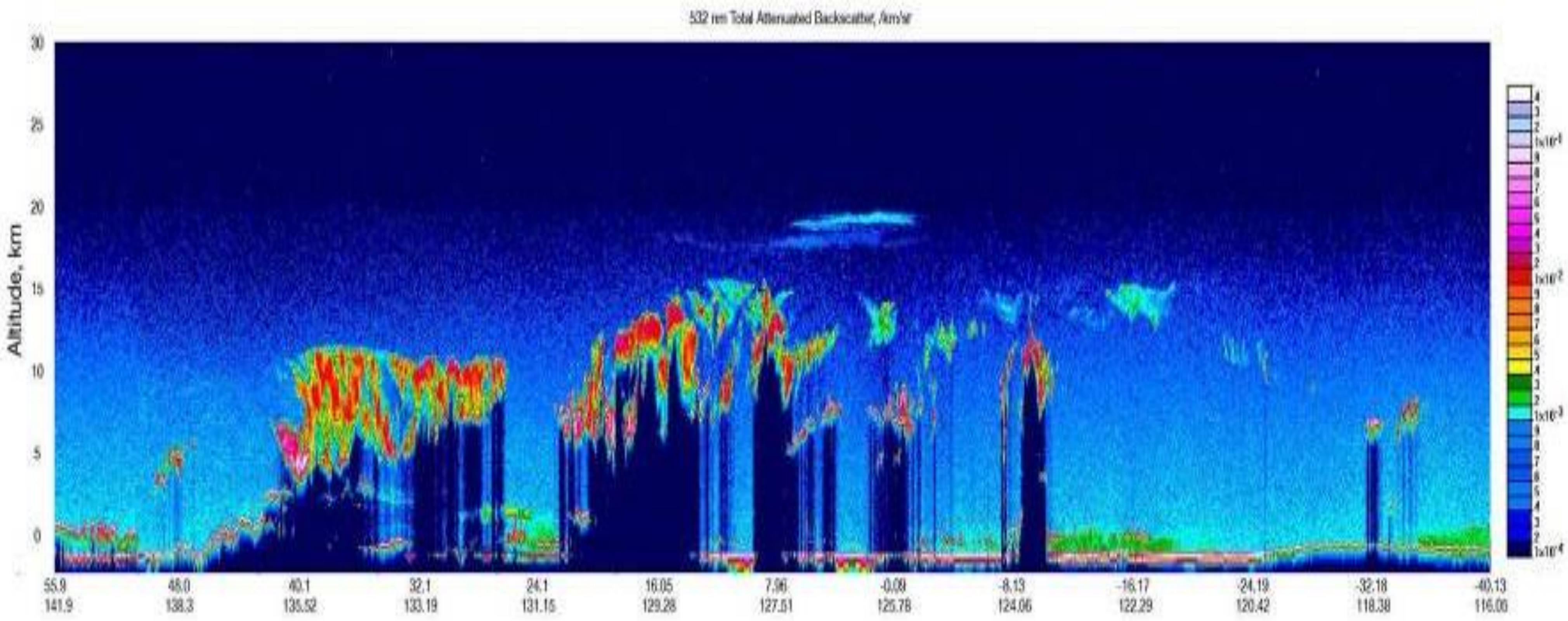

Georgia Tech Research Institute

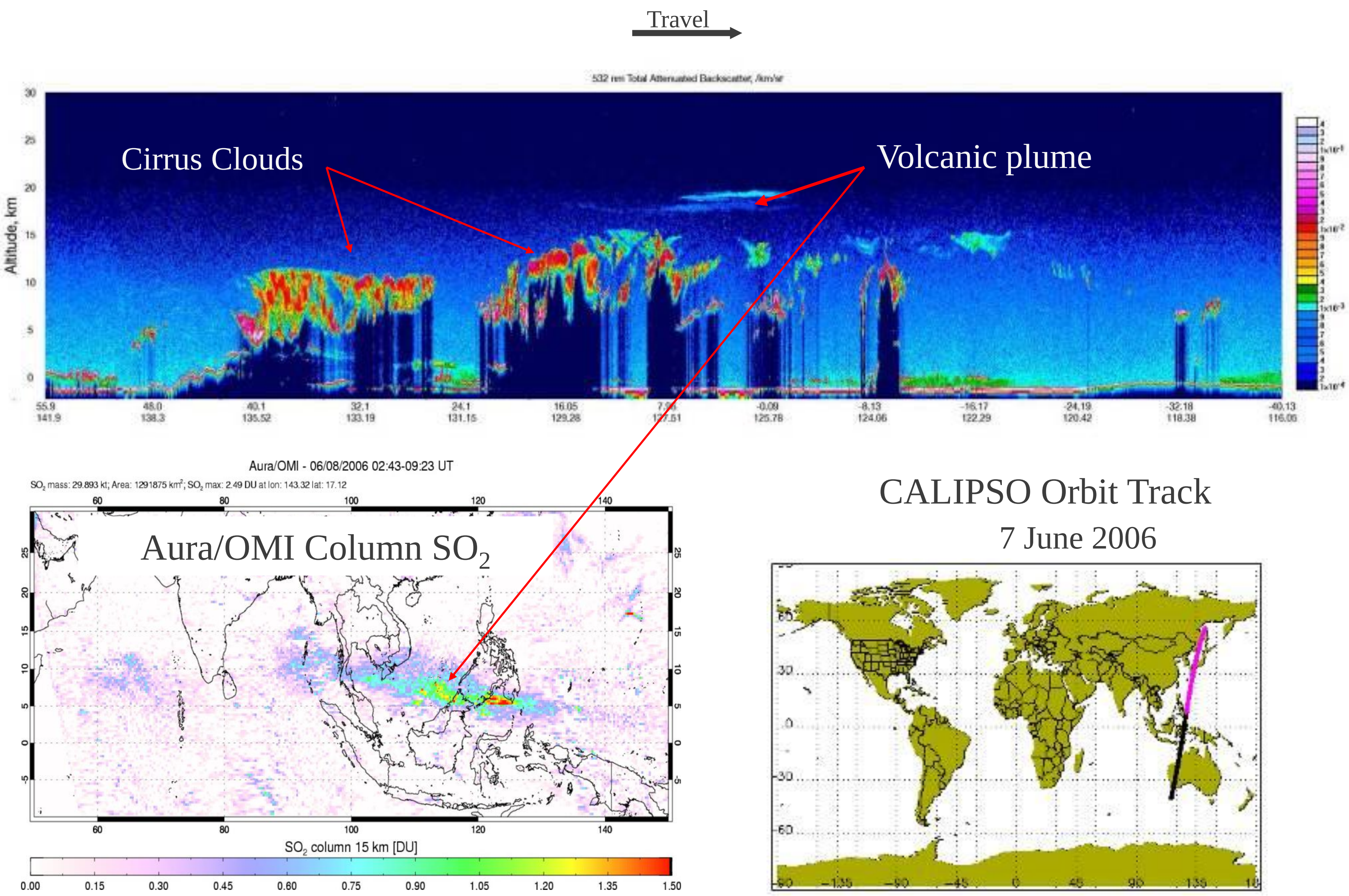

Soufriere (Montserrat – Caribbean) erupted on May 20. Its water droplet/sulfuric acid plume was tracked by OMI and seen crossing over Indonesia by CALIPSO on June 7.

From Dr. Irina Sokolik's *Remote Sensing of the Atmosphere and Oceans* course

Georgia Tech Research Institute

Overview

- Atmospheric Lidar Theory
- History of Lidar for Atmospheric Study
- Recent Developments

Overview

- **Atmospheric Lidar Theory**
- History of Lidar for Atmospheric Study
- Recent Developments

Basic Lidar system:
The Elastic Backscatter Lidar

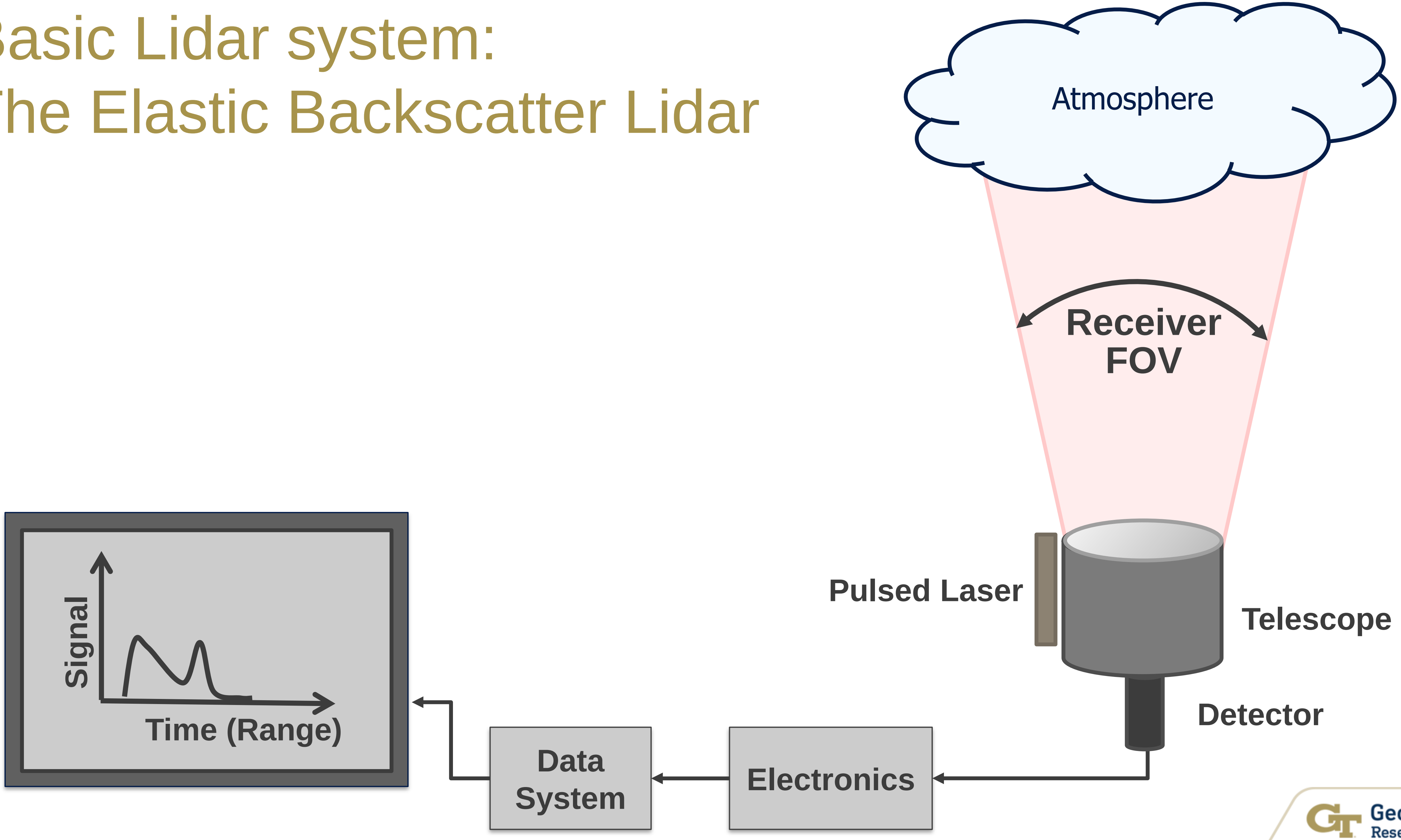

Basic Lidar system:
The Elastic Backscatter Lidar

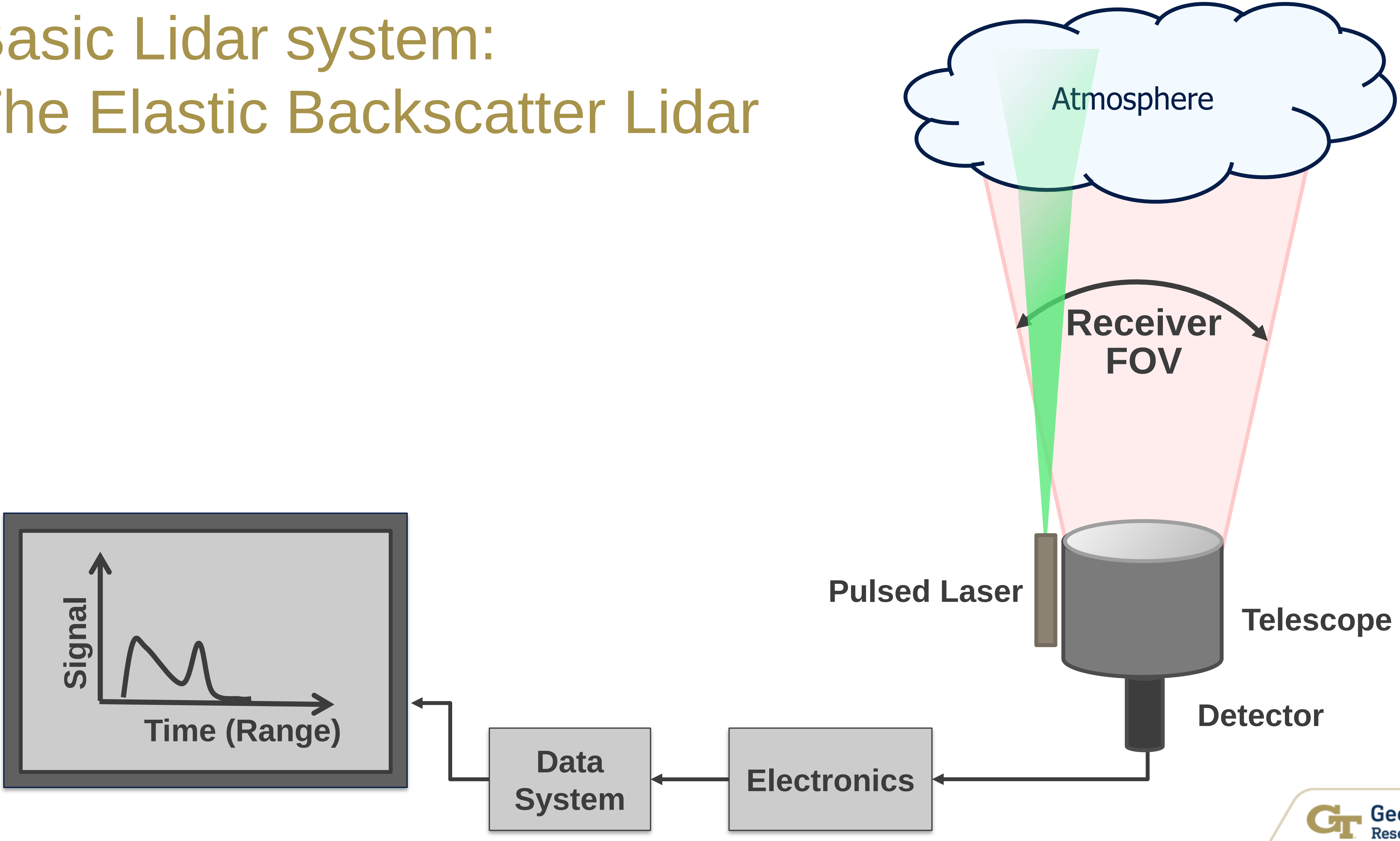

Basic Lidar system:
The Elastic Backscatter Lidar

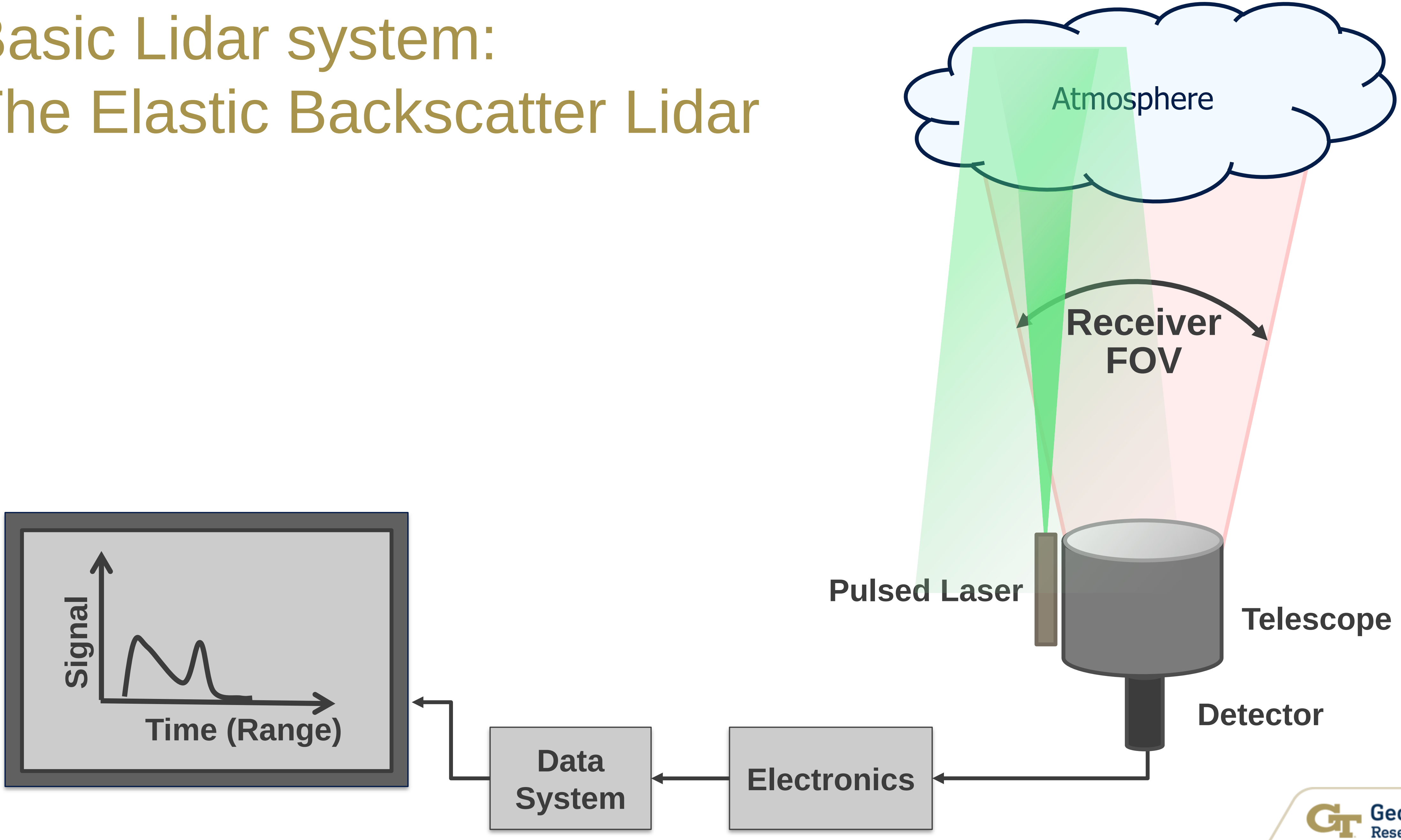

Georgia Tech Research Institute

Sky background

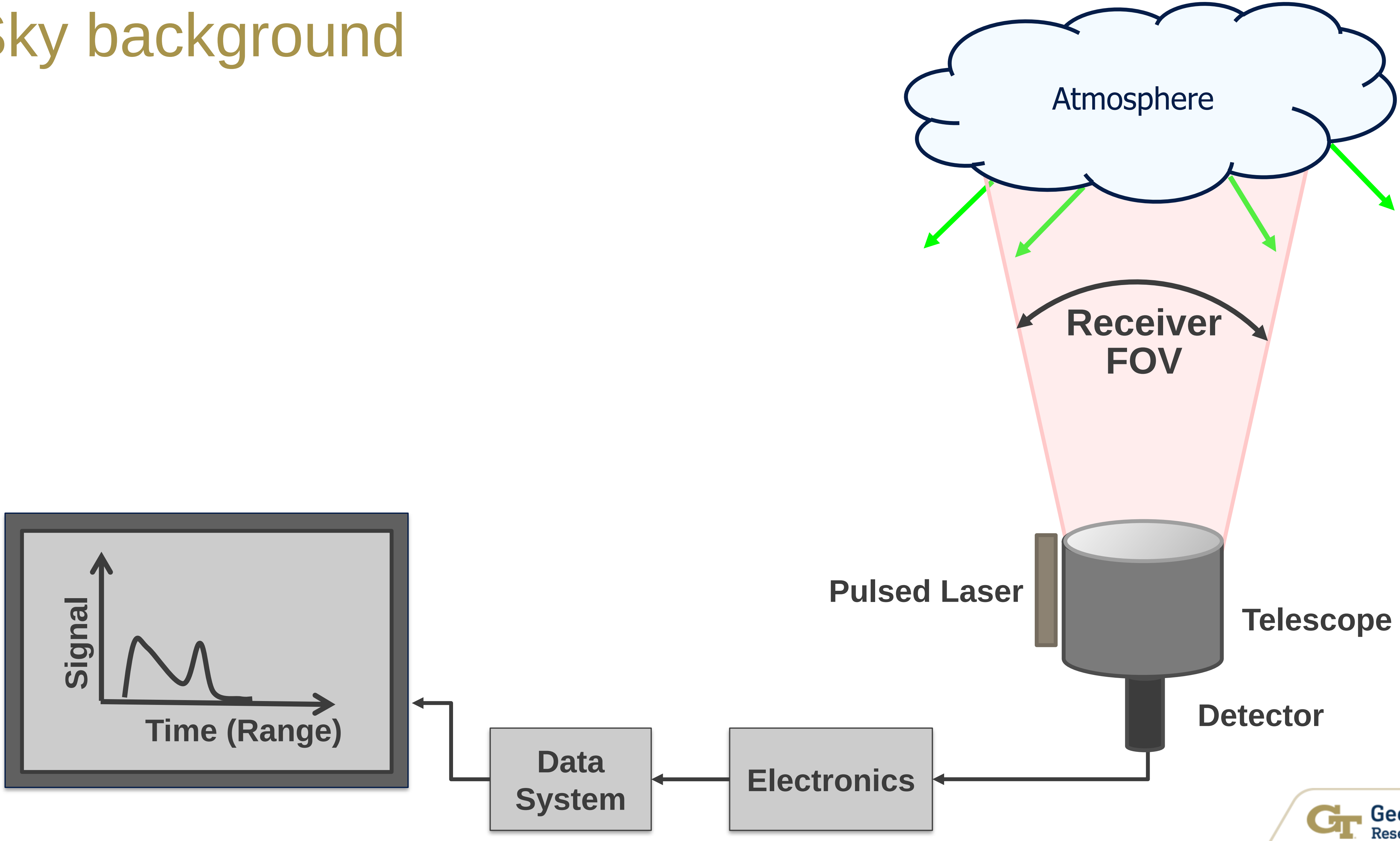

Components of the Lidar Equation

The power received from a range bin is proportional to:

- **Power** transmitted, P_0
- **Transmitter and receiver optical efficiency**, k_t and k_{rec}
- **Receiver collecting area**, A_{rec}
- A range-dependent **geometrical overlap factor** (not shown in figure), G(r)
- The range bin **backscatter coefficient**, β
- The length of the **range bin**, ct/2
- The atmospheric **transmittance** to & from the range bin, T_{path}

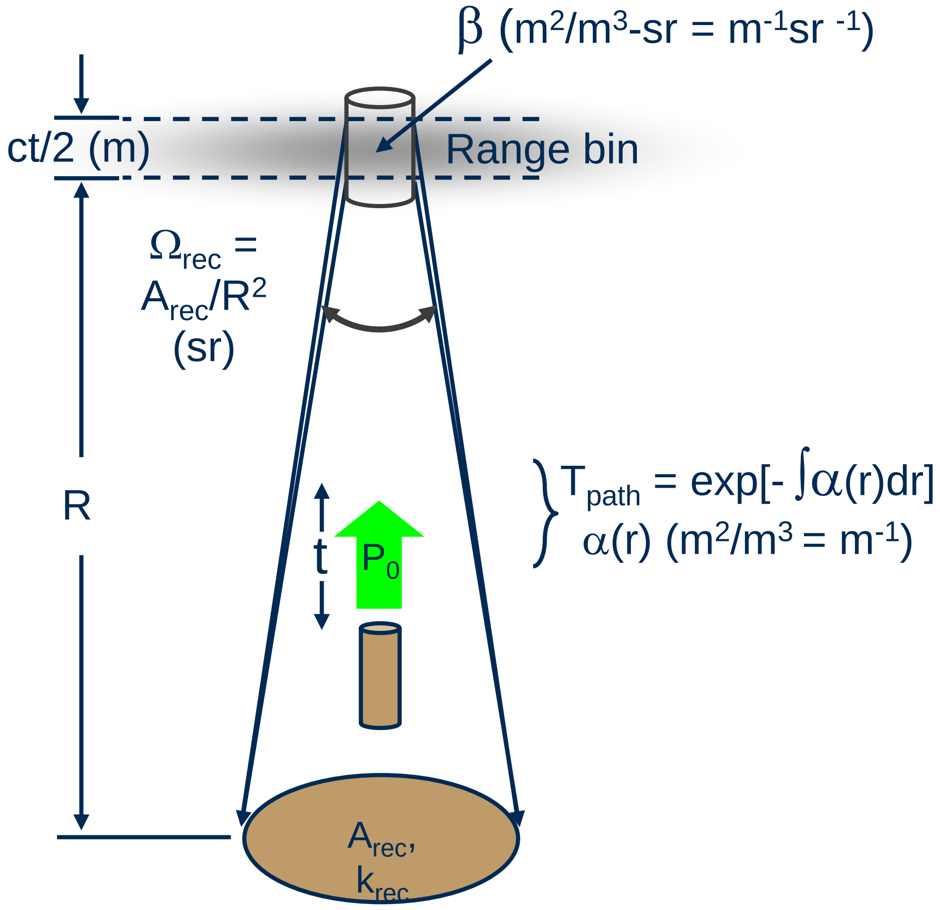

The Elastic Backscatter Lidar equation

$$P_L(R) = P_o\,\eta_T\,\eta_R\,G(R)\left(\frac{A}{R^2}\right)\left(\frac{ct}{2}\right)\beta(R)\exp\left[-2\int_0^R \alpha(R')dR'\right]$$

$P_L(R) =$ Power received from range, R

$P_o =$ Average power per laser pulse

$\eta_T =$ Transmitter optical efficiency

$\eta_R =$ Receiver optical efficiency

$G(R) =$ Geometric overlap factor

$\left(\frac{A}{R^2}\right) =$ Receiver solid angle (sr)

$\left(\frac{ct}{2}\right) =$ Range bin length (m)

$\beta(R) =$ Atmos. Volume backscatter coefficient ($m^{-1}sr^{-1}$)

$\exp\left[-2\int_0^R \alpha(R')dR'\right] =$ Two-way path transmittance

$\alpha(R) =$ Atmos. extinction coefficient (m^{-1})

The Elastic Backscatter Lidar equation

$$\boxed{P_L(R)} = P_o\, \eta_T\, \eta_R\, G(R) \left(\frac{A}{R^2}\right)\left(\frac{ct}{2}\right)\beta(R)\exp\left[-2\int_0^R \alpha(R')dR'\right]$$

Power received per range bin

$P_L(R)$ = Power received from range, R

P_o = Average power per laser pulse

η_T = Transmitter optical efficiency

η_R = Receiver optical efficiency

$G(R)$ = Geometric overlap factor

$\left(\frac{A}{R^2}\right)$ = Receiver solid angle (sr)

$\left(\frac{ct}{2}\right)$ = Range bin length (m)

$\beta(R)$ = Atmos. Volume backscatter coefficient ($m^{-1}sr^{-1}$)

$\exp\left[-2\int_0^R \alpha(R')dR'\right]$ = Two-way path transmittance

$\alpha(R)$ = Atmos. extinction coefficient (m^{-1})

Georgia Tech Research Institute

The Elastic Backscatter Lidar equation

Power transmitted

$$\boxed{P_L(R)} = \boxed{P_o}\,\eta_T\,\eta_R\,G(R)\left(\frac{A}{R^2}\right)\left(\frac{ct}{2}\right)\beta(R)\exp\left[-2\int_0^R \alpha(R')dR'\right]$$

Power received per range bin

$P_L(R)$ = Power received from range, R

P_o = Average power per laser pulse

η_T = Transmitter optical efficiency

η_R = Receiver optical efficiency

$G(R)$ = Geometric overlap factor

$\left(\frac{A}{R^2}\right)$ = Receiver solid angle (sr)

$\left(\frac{ct}{2}\right)$ = Range bin length (m)

$\beta(R)$ = Atmos. Volume backscatter coefficient ($m^{-1}sr^{-1}$)

$\exp\left[-2\int_0^R \alpha(R')dR'\right]$ = Two-way path transmittance

$\alpha(R)$ = Atmos. extinction coefficient (m^{-1})

The Elastic Backscatter Lidar equation

Photons transmitted

$$\boxed{P_L(R)} = \boxed{P_o}\, \eta_T\, \eta_R\, G(R) \left(\frac{A}{R^2}\right)\left(\frac{ct}{2}\right) \beta(R) \exp\left[-2\int_0^R \alpha(R')\,dR'\right]$$

Power received per range bin

System variables

$P_L(R)$ = Power received from range, R

P_o = Average power per laser pulse

η_T = Transmitter optical efficiency

η_R = Receiver optical efficiency

$G(R)$ = Geometric overlap factor

$\left(\frac{A}{R^2}\right)$ = Receiver solid angle (sr)

$\left(\frac{ct}{2}\right)$ = Range bin length (m)

$\beta(R)$ = Atmos. Volume backscatter coefficient ($m^{-1}sr^{-1}$)

$\exp\left[-2\int_0^R \alpha(R')\,dR'\right]$ = Two-way path transmittance

$\alpha(R)$ = Atmos. extinction coefficient (m^{-1})

The Elastic Backscatter Lidar equation

Photons transmitted | **Atmospheric variables**

$$\boxed{P_L(R)} = \boxed{\boxed{P_o}\,\eta_T\,\eta_R\,G(R)\left(\frac{A}{R^2}\right)\left(\frac{ct}{2}\right)}\,\boxed{\beta(R)\exp\left[-2\int_0^R \alpha(R')\,dR'\right]}$$

Power received per range bin

System variables

$P_L(R)$ = Power received from range, R

P_o = Average power per laser pulse

η_T = Transmitter optical efficiency

η_R = Receiver optical efficiency

$G(R)$ = Geometric overlap factor

$\left(\frac{A}{R^2}\right)$ = Receiver solid angle (sr)

$\left(\frac{ct}{2}\right)$ = Range bin length (m)

$\beta(R)$ = Atmos. Volume backscatter coefficient ($m^{-1}sr^{-1}$)

$\exp\left[-2\int_0^R \alpha(R')\,dR'\right]$ = Two-way path transmittance

$\alpha(R)$ = Atmos. extinction coefficient (m^{-1})

Elastic Backscatter Equation Assumptions

- The backscattered light is at the same wavelength as the transmitted light
- All range-dependent signal losses apart from the $1/R^2$ factor are due to the atmosphere, not the technology
- Photons experience a single scattering event during their trip through the atmosphere - no multiple scattering
- The entire laser pulse is contained within the range bin
- α and β are constant within a range bin
- Only one laser pulse at a time is in the atmosphere

$\alpha(R)$ & $\beta(R)$ – Extinction and Backscatter Coefficients

Extinction and backscatter coefficients have components from interactions with **aerosols** and **molecules**:

$$\alpha(R) = \alpha_{aero} + \alpha_{mol}$$

$$\beta(R) = \beta_{aero} + \beta_{mol}$$

Atmospheric extinction is due to **absorption** and **scattering**:

$$\alpha(R) = \alpha_{aero,\,abs} + \alpha_{aero,\,sca} + \alpha_{mol,\,abs} + \alpha_{mol,\,sca}$$

- The terms $\beta(z)$ and $\alpha(z)$ are the range-dependent parameters of interest for atmospheric studies
- The molecular scattering quantities are proportional to atmospheric number density (N_2, O_2, Ar)
- Unfortunately, they represent several unknowns in a single equation
  - An underdetermined system (on its own!)

The Challenge

- The lidar equation describes one signal that depends on two atmospheric parameters, in different ways.
  - There is no unique solution
  - We must either reduce the number of parameters to one by:
    - Defining $S_a = \alpha/\beta$, (so $\alpha = S_a\beta$) or
    - Using Rayleigh β in aerosol-free regions to calibrate, or
    - Working in the mesosphere where $\alpha \sim 0$,
  - Or add more information:
    - From other instruments
    - Using Two (or more) wavelengths, angles, polarizations, etc.
  - Much of the history of LIDAR describes efforts to overcome this challenge!

Rayleigh Lidar (Upper Atmospheric Lidar)

- **Rayleigh lidar** essentially bypasses the lower atmosphere and only receives useful signal from >30 km where aerosols are typically not present (Hauchecorne and Chanin; 1980)
  - Measurements include: temperature, density, dynamics (gravity waves, tides, planetary waves)
- **Resonance fluorescence lidar** transmitted light is matched to a specific atomic transition or electronic transition of a specific atom (Bowman et al., 1969)
  - Upper atmospheric species studied: sodium, iron, potassium, calcium/calcium ion, nickel
- Limits studies to upper atmosphere

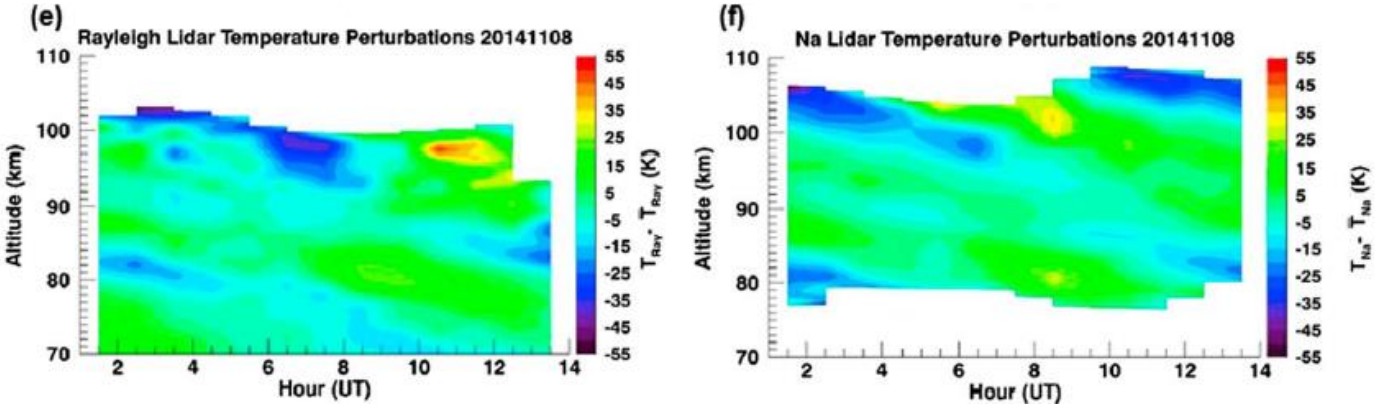

Sox et al., 2018

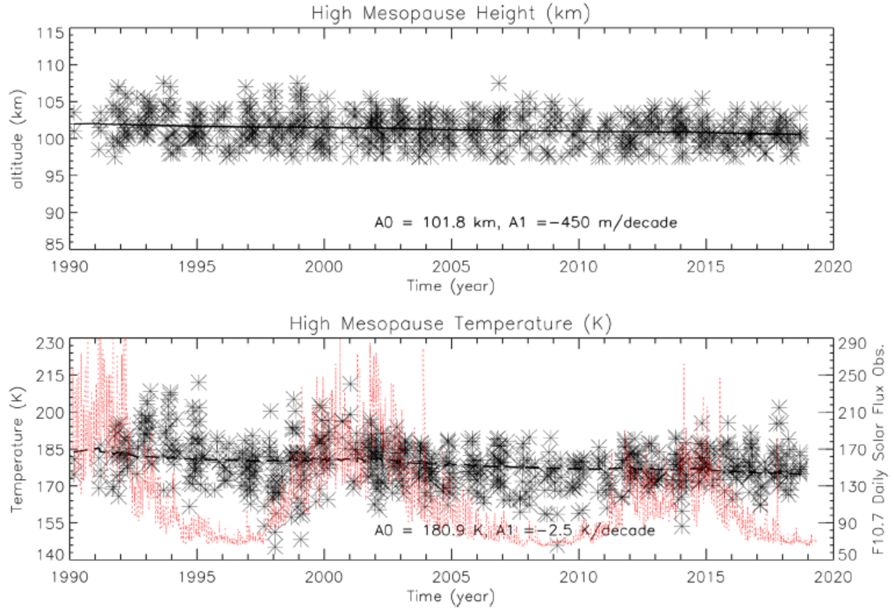

Figure 3. The long-term variations of (top) mesopause height and (bottom) temperature trend of the lidar-measured nonsummer high mesopause, along with their constant, A0, and linear (A1) terms derived from the trend regression.

Yuan et al., 2019

Georgia Tech Research Institute

Fernald-Klett Data Analysis Method

- The Fernald-Klett algorithm is a **data analysis** method for retrieving aerosol extinction from lidar signal (Fernald et al., 1972; Fernald, 1984; Klett, 1981)
- Inversion technique, which requires additional information:
  - Estimated or modeled molecular extinction profile
  - Initial value of aerosol extinction at maximum range
  - Initial guess of the lidar aerosol extinction-to-backscatter ratio, $S_a = \frac{\alpha_a}{\beta_a}$
  - Auxiliary measurement to constrain the inversion (e.g. sun photometer aerosol optical depth measurement)
- This method is still widely used in modern atmospheric lidar programs like NASA's Micro-Pulse Lidar NETwork (MPLNET; Welton et al., 2001)

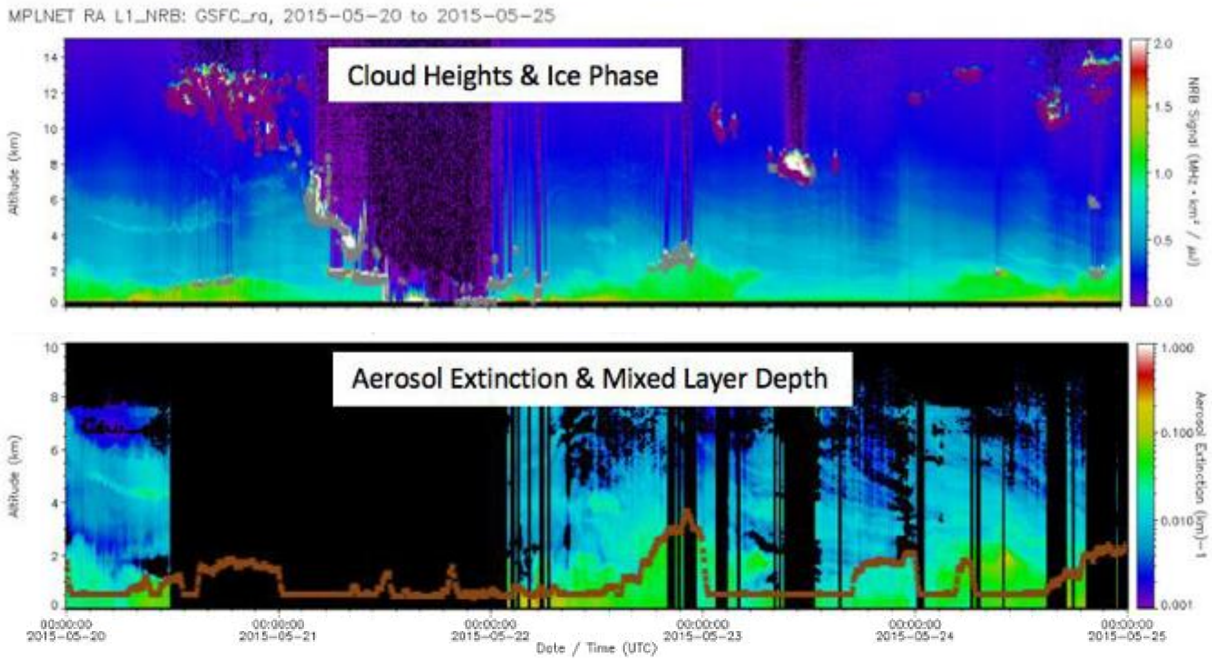

Figure 3. MPLNET V3 Cloud, Aerosol and PBL Products

Welton et al., 2018

Depolarization and Multi-Wavelength Lidar

- Can add further **hardware capabilities** to distinguish aerosol types
- Depolarization lidar measures degree to which the received light's polarization state has changed from the transmitter laser light
  - Lower depolarization → atmospheric scatterers are spherical
  - Higher depolarization → atmospheric scatterers are non-spherical
- Adding multiple wavelengths gives more information about particle sizes

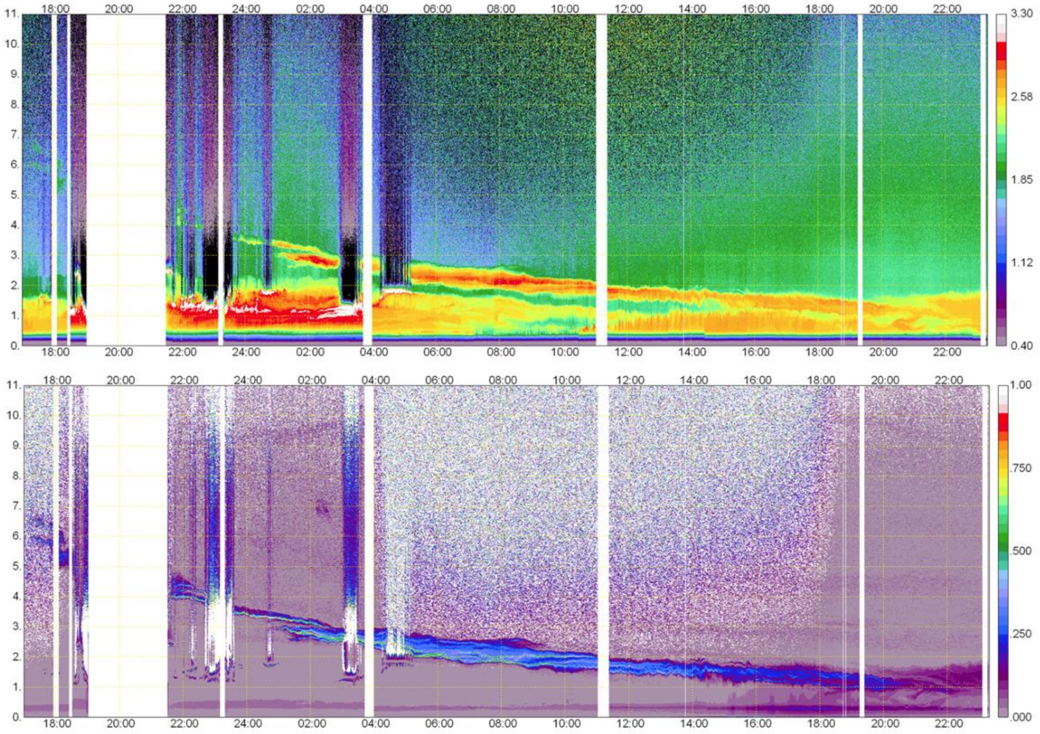

Fig. 1. Time–height cross section of the range-corrected signal (upper panel, log-scale, a.u.) and the volume linear depolarization ratio (lower panel) at 532 nm derived from MULIS lidar measurements at Maisach from 16 April 17 UTC to 17 April 24 UTC.

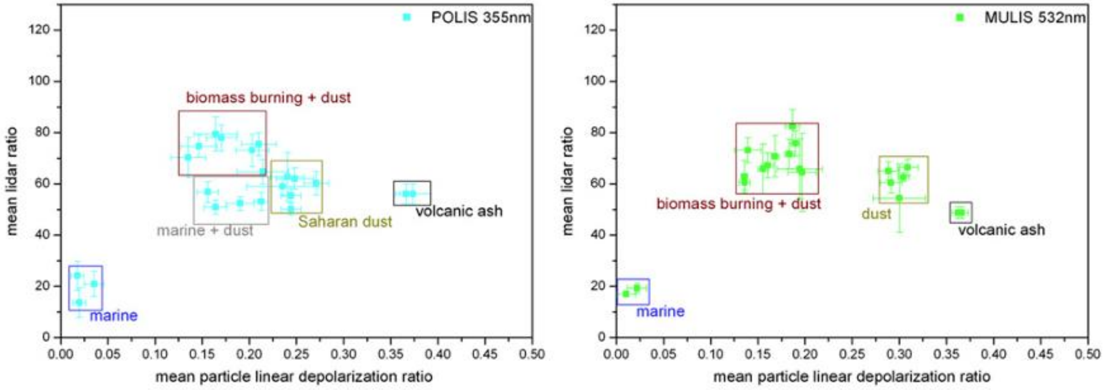

Fig. 14. Particle lidar ratio vs. particle linear depolarization ratio for different aerosol types at 355 nm (left) and 532 nm (right).

Groß et al., 2012

Georgia Tech Research Institute

Differential Absorption Lidar (DIAL)

- **Transmit two different wavelengths** that have distinct absorption cross-sections (σ) for the interrogated trace gas
  - Identify "on" and "off" wavelengths for selected trace gas, difference of cross sections proportional to difference in atmospheric extinction:

$$\Delta\alpha = \rho_{trace\ gas}\,\Delta\sigma$$

$$\rho_{trace\ gas} = \frac{1}{2\Delta\sigma}\left[\frac{d}{dR}\ln\left(\frac{P_{on}}{P_{off}}\right)\right]$$

- Mostly used to measure trace gas concentrations: ozone, methane, water vapor, etc.

- Recent work has demonstrated DIAL system for temperature measurements (Stillwell et al., 2020)

Gimmestad, 2005

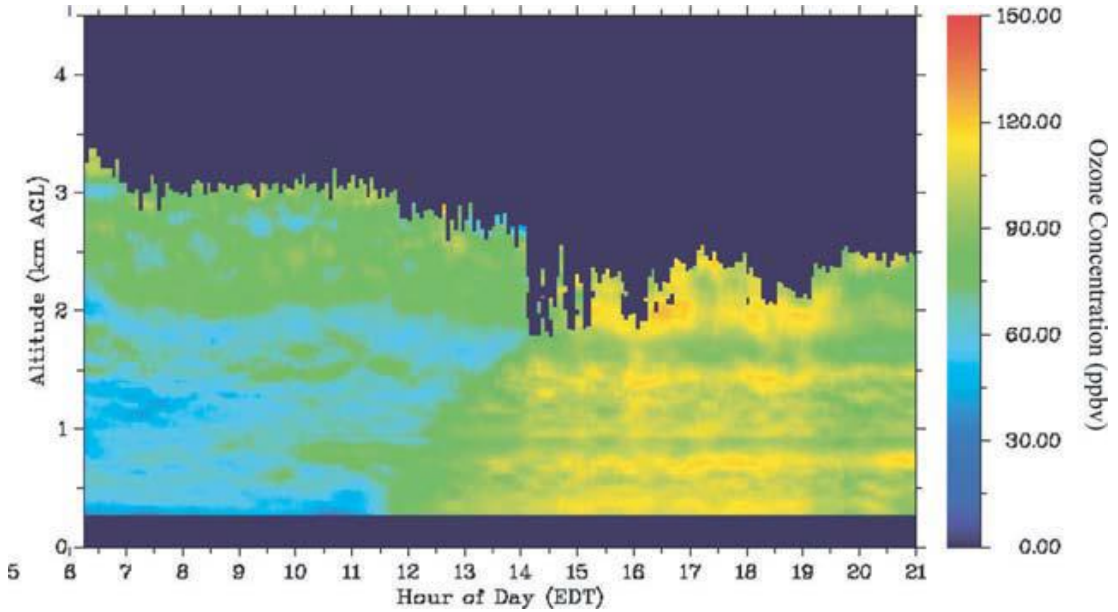

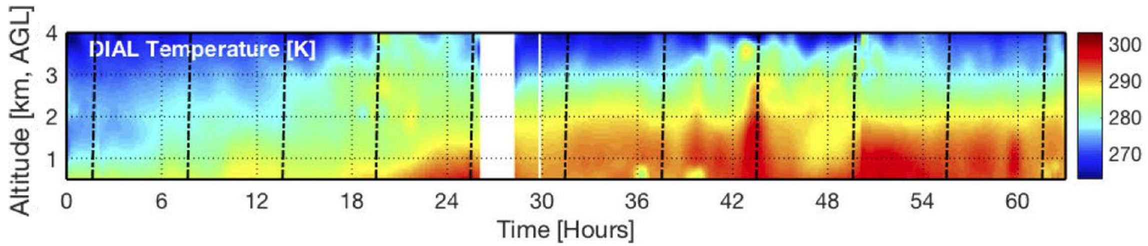

Stillwell, 2020

Raman lidar

- Raman lidar creates a source at a new wavelength, in the scattering volume, by inelastic scattering molecular species
  - – The Raman backscatter is much weaker than Rayleigh
- Raman lidars designed to **receive two or more shifted wavelengths**
- Raman lidar technique can be used to spectroscopically separate molecular and aerosol extinction
- Technique can also be used to measure:
  - – Vibrational-rotational Raman: Trace gas concentrations (water vapor, methane, carbon dioxide)
  - – Rotational Raman: Temperature

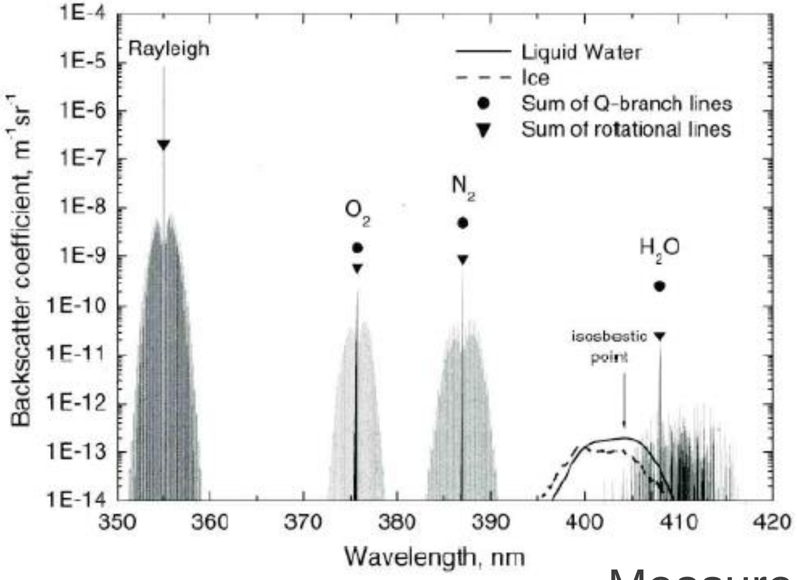

Measures, 1994

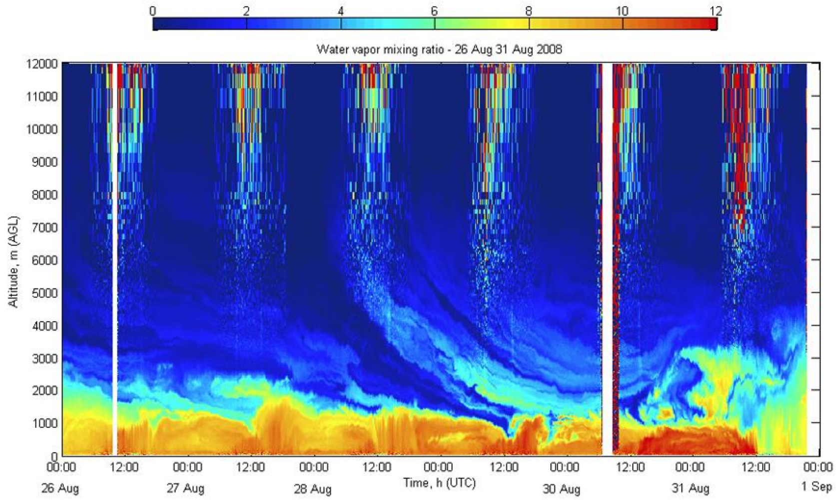

Fig. 14. Six-day time series of water vapor with 10 min time resolution. All data are shown, including data with a statistical error > 10 %. The noisy zones above 5000 m (around noon) mark the increase in statistical error due to the solar background during the daytime. The white zones mark data gaps.

Dinoev et al., 2013

High Spectral Resolution Lidar (HSRL)

- HSRL technique optically separates Rayleigh (molecular) and Mie (aerosol) signals (Shipley, 1983)
- Spectral distribution of molecular signal is Doppler-broadened, aerosol spectral distribution is not broadened
  - An atomic-vapor filter is used to block the aerosol signal so that the molecular and aerosol signals can be separated
- Returned signal separated into two channels:
  - Molecular backscatter channel
  - Molecular + aerosol backscatter channel
- Profile of molecular density is modeled/measured from auxiliary instruments is required to calibrate

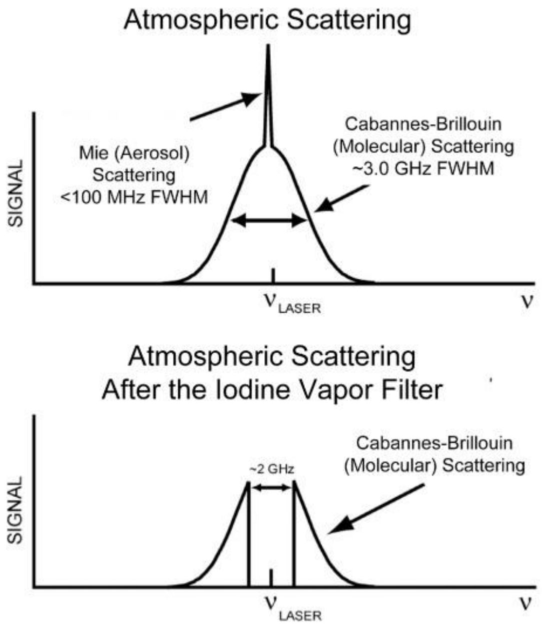

Hair et al., 2008

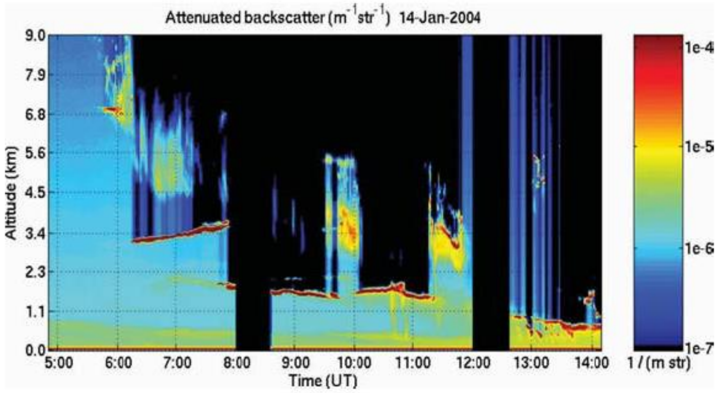

Fig. 5.6. Attenuated backscatter image recorded with the HSRL on 14 January 2004.

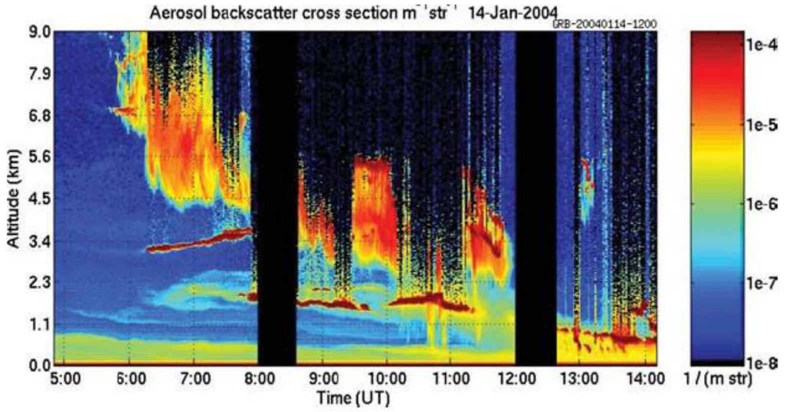

Fig. 5.7. Aerosol backscatter coefficient recorded on 14 January 2004.

Eloranta, 2005

Doppler Wind Lidar

- Typically achieved with **coherent detection**: atmospheric backscatter signal, is mixed with a local oscillator reference beam (Pearson et al., 2009)
- Doppler shifts are determined from the spectrum of the mixed signal
- Most systems are built to scan and measure line-of-sight velocities at each pointing angle in the scan
  - LOS winds can be decomposed into 3D components
- Commercial systems widely available (Halo Photonics, Vaisala)

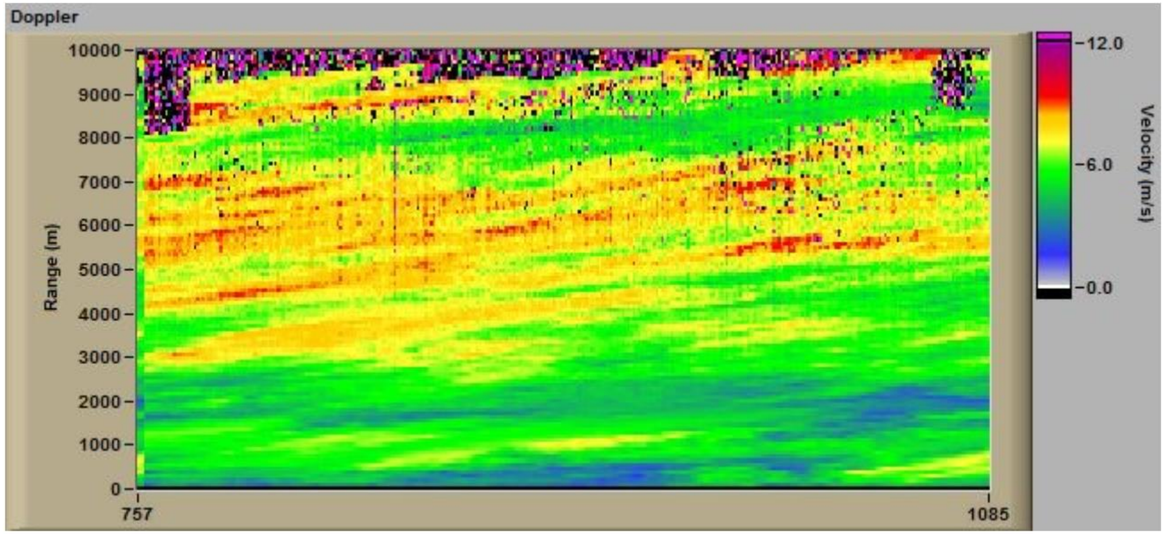

Range/time/Doppler plot for a fixed LOS 40 m gates, 1-second average per ray, 6-minute record. The raw data were saved and re-processed as shown below.

https://halo-photonics.com/lidar-systems/streamline-allsky-series/

Lidar Design

- There are many different types lidar to choose from!

- Lidar performance is affected by many atmospheric, optical, electronic, mechanical, algorithmic, and geometric factors

- High-fidelity atmospheric lidar simulator coupled with Monte Carlo analysis has been developed to aid in lidar system design and algorithm development (Valenta & Sox, 2022)

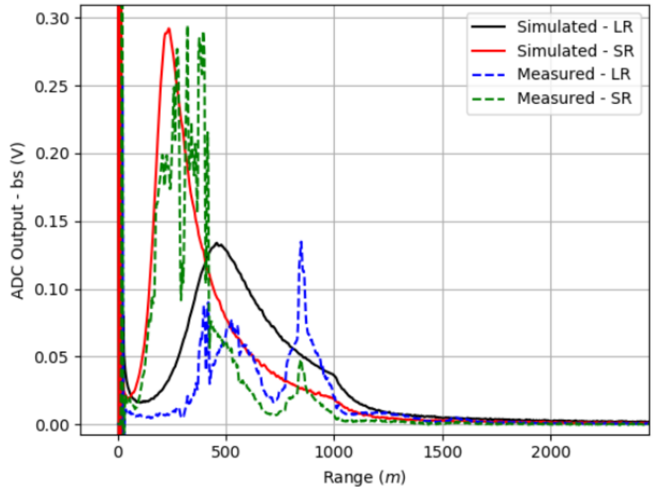

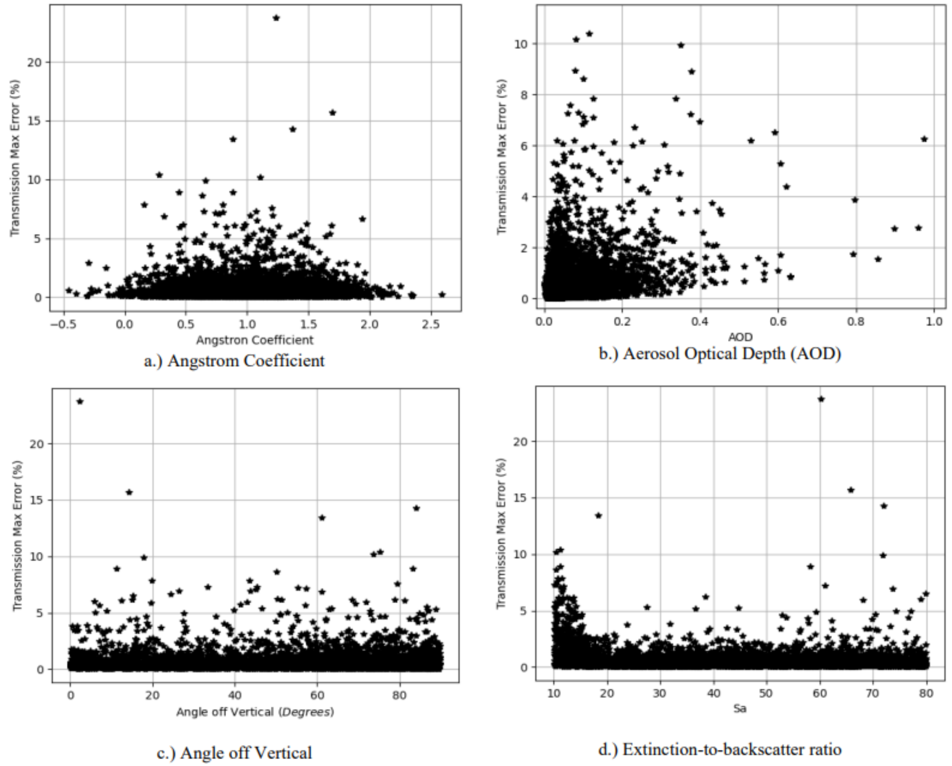

Figure 14. Transmission error Monte Carlo results while varying the a.) Angstrom coefficient b.) aerosol optical depth (AOD), c.) angle off vertical, and d.) aerosol extinction-to-backscatter ratio.

Valenta & Sox, 2022

Georgia Tech Research Institute

Overview

- Atmospheric Lidar Theory
- **History of Lidar for Atmospheric Study**
- Recent Developments

Searchlight Lidar

- Lidar technique first proposed by Sygne, 1930 to measure atmospheric scatter from searchlight beams

- First measurements came from bistatic searchlight systems (e.g. Hulbert, 1937)

- Johnson et al., (1939) showed profile of atmospheric structure with respect to altitude using a "pulsed" system

Johnson et al., 1939

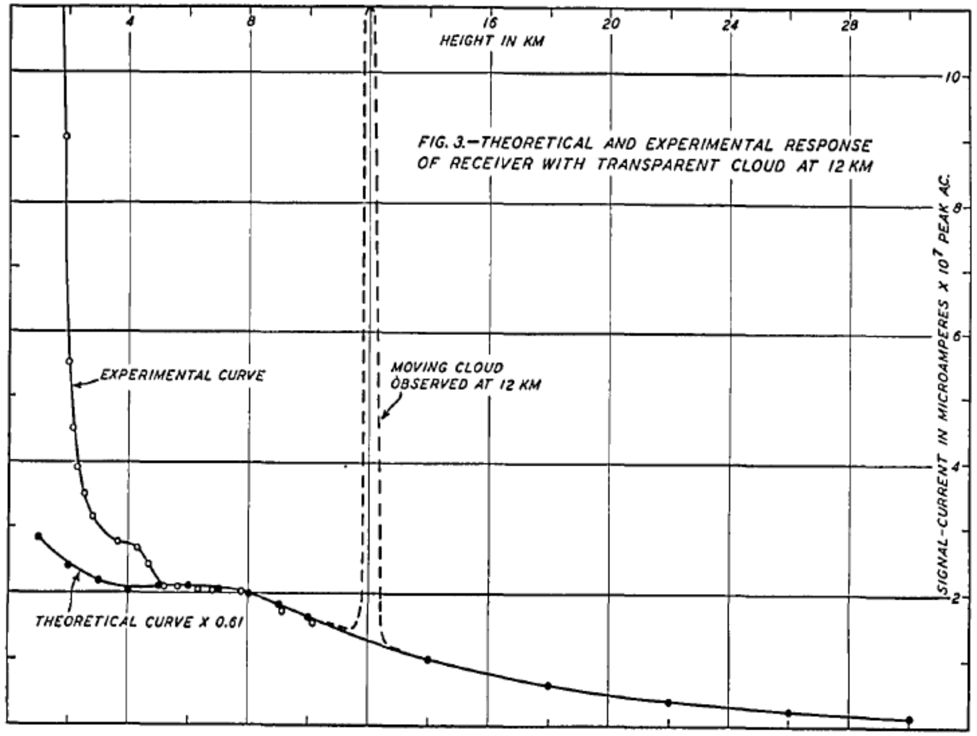

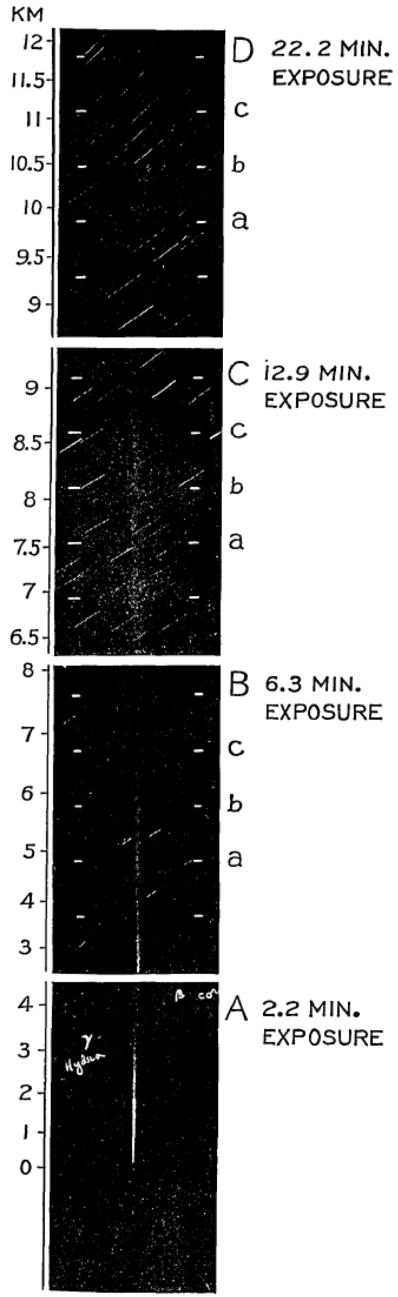

Hulbert, 1937

1930s	1960	1963	1960-1990s	2000s	2006	2018
Lidar with searchlights	First Laser	First Lidar	Lidar Techniques Developed	Lidar Networks	NASA CALIPSO	ESA Aeolus

Georgia Tech Research Institute

First Ruby Lidar

- First working laser in 1960 (Maiman, 1960)
- Fiocco & Smullin demonstrated first ruby laser-based atmospheric lidar in 1963

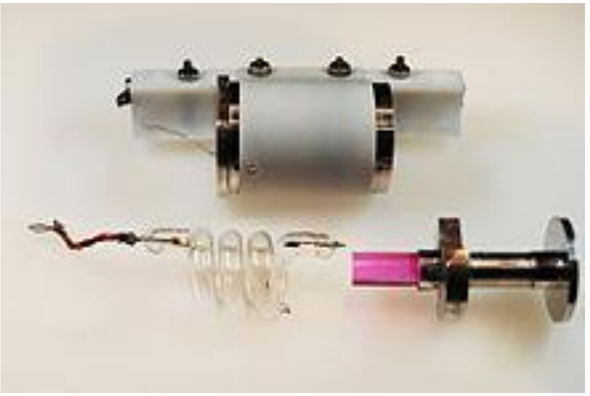

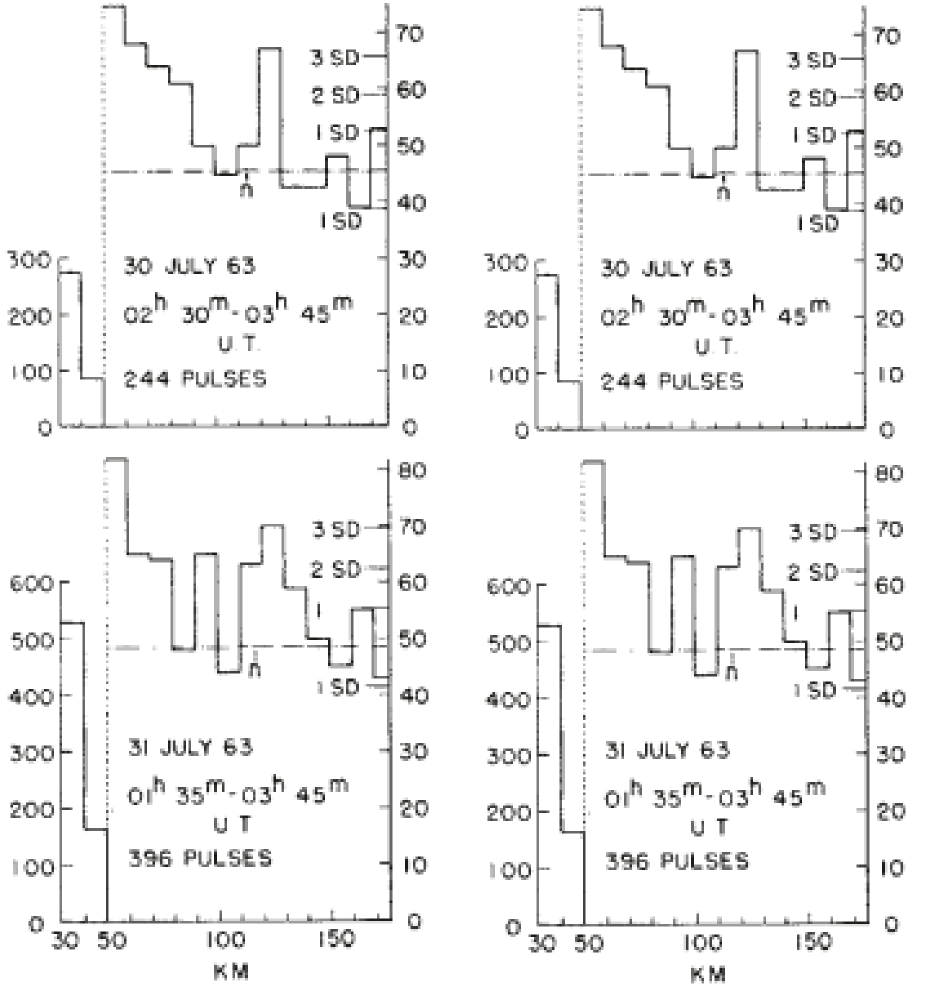

Fiocco & Smullin, 1963

Lidar with searchlights	**First Laser**	**First Lidar**	Lidar Techniques Developed	Lidar Networks	NASA CALIPSO	ESA Aeolus
1930s	**1960**	**1963**	1960-1990s	2000s	2006	2018

Many Lidar Techniques

- Many atmospheric lidar techniques were developed after the first system came online:
  - **Rayleigh lidar** ~1960s-1980s: Hauchecorne & Chanin, 1980
  - **Raman lidar** ~1960s-1970s: Leonard & Caputo, 1974; Cooney
  - **DIAL** ~ 1960s-1970s: Schotland, 1966
  - **HSRL** ~ 1980s: Shipley et al., 1984

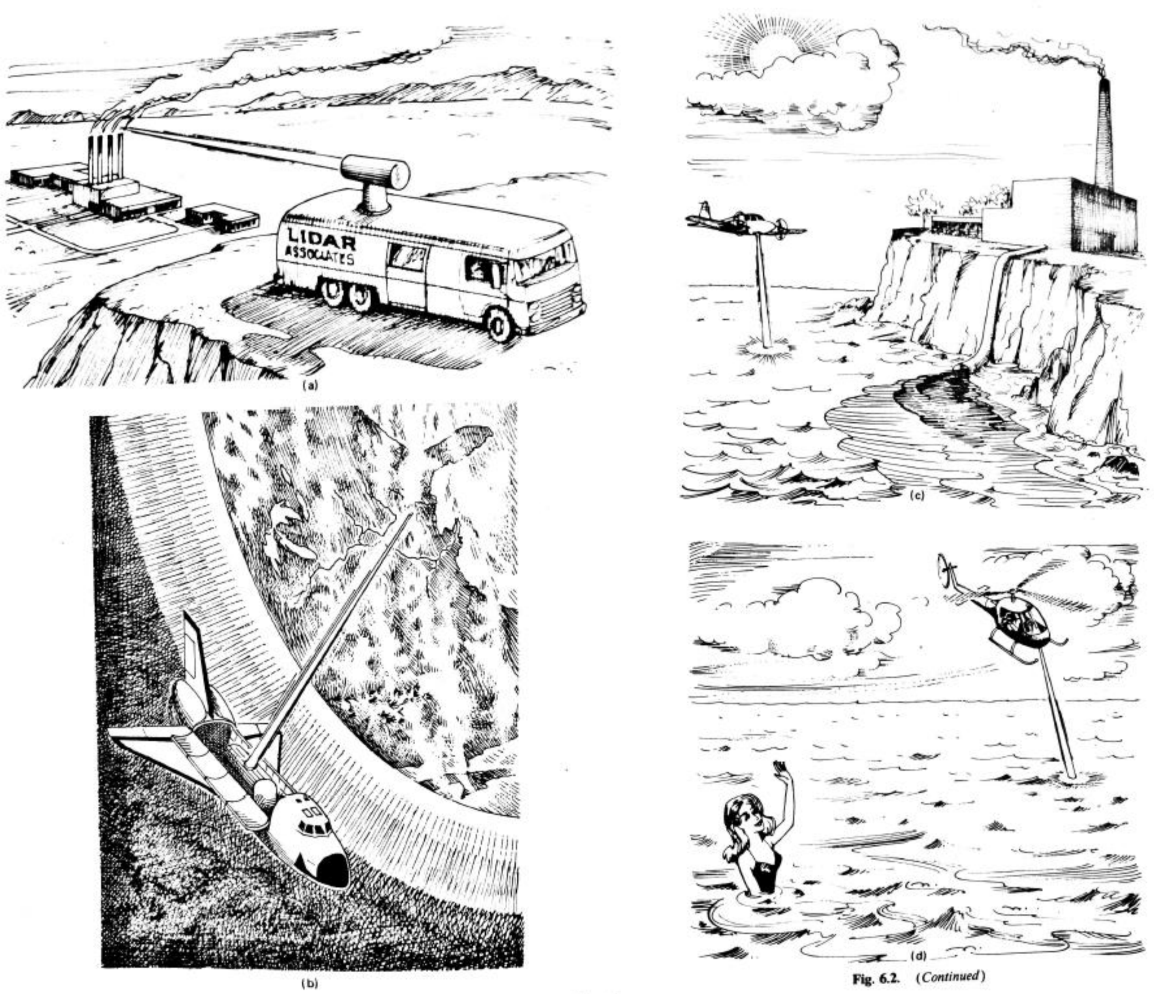

Measures, 1994

Lidar with searchlights	First Laser	First Lidar	**Lidar Techniques Developed**	Lidar Networks	NASA CALIPSO	ESA Aeolus
1930s	1960	1963	**1960-1990s**	2000s	2006	2018

Georgia Tech Research Institute

Ground-based Lidar Networks

- NASA Micro-Pulse Lidar Network (MPLNET)
  - ~26 active Micro-pulse elastic backscatter lidars with depolarization functionality
- NASA Tropospheric Ozone Lidar Network (TOLNET)
  - ~6 DIAL Ozone lidars (Leblanc et al., 2018)
- European Aerosol Research Lidar Network (EARLINET)
  - 30+ elastic and multi-wavelength Raman lidars (Pappalardo et al., 2014)

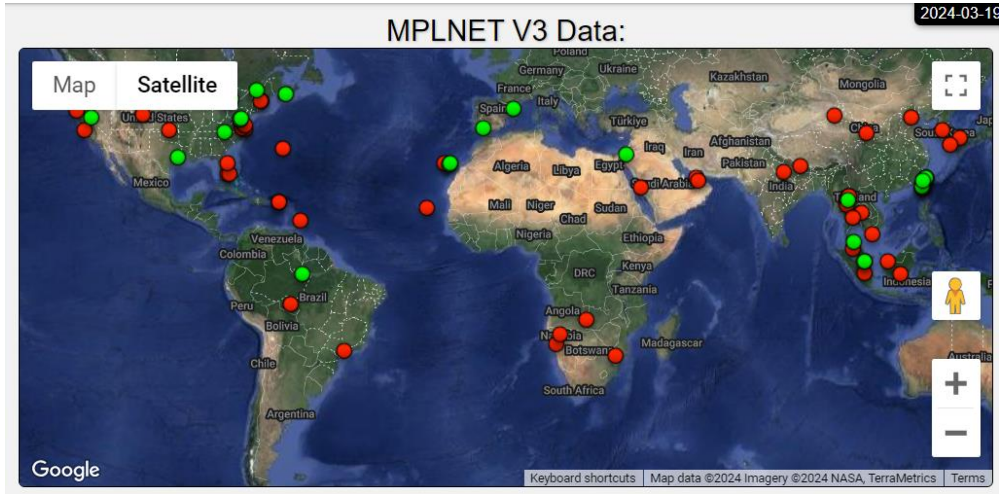

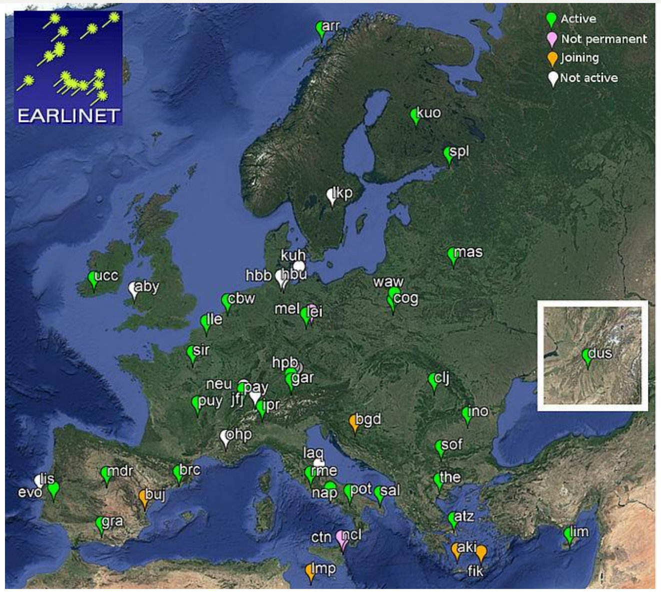

Lidar with searchlights	First Laser	First Lidar	Lidar Techniques Developed	**Lidar Networks**	NASA CALIPSO	ESA Aeolus
1930s	1960	1963	1960-1990s	**2000s**	2006	2018

Georgia Tech Research Institute

Lidars in Space!

Omar et al., 2009

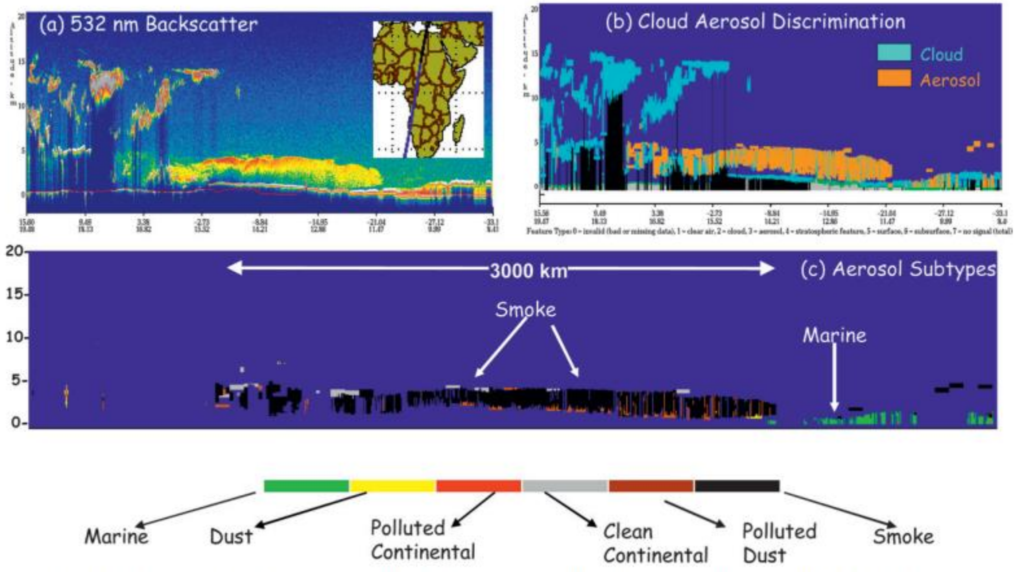

FIG. 4. (a) A 532-nm backscatter browse image, (b) cloud–aerosol mask, and (c) the corresponding aerosol subtyping plot showing vast smoke layer in southwestern Africa during the peak of the burning season, observed on 8 Aug 2006 and stretching across land into the South Atlantic. The relative scales are as in Fig. 3.

- NASA/CNES Cloud-Aerosol Lidar with Orthogonal Polarization (CALIOP) onboard the CALIPSO satellite
  - Launched in 2006, ended 2023
  - Elastic backscatter lidar with depolarization and two wavelengths

- ESA Atmospheric Laser Doppler Instrument (ALADIN) onboard Atmospheric Dynamics Mission-Aeolus satellite
  - Launched in 2018, ended 2023
  - Doppler wind lidar for winds from 0-30 km

ESA/ECMWF:http://m.esa.int/spaceimages/Images/2018/09/Winds_imaged_by_Aeolus

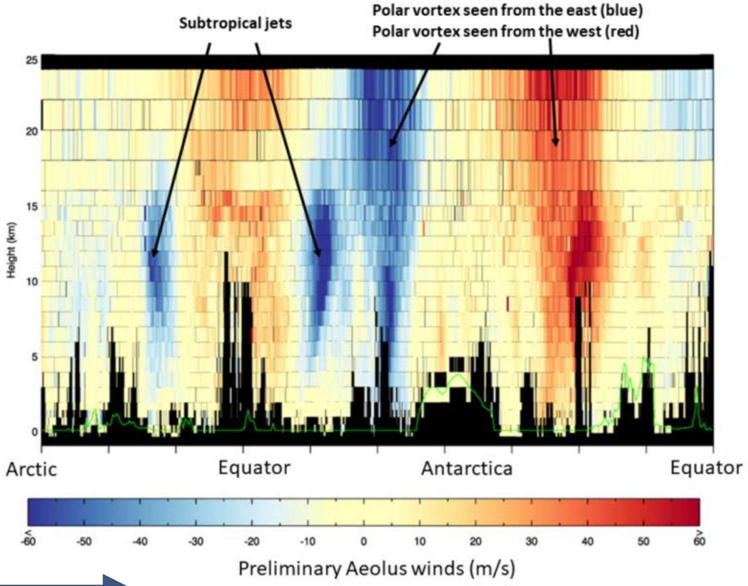

Lidar with searchlights	First Laser	First Lidar	Lidar Techniques Developed	Lidar Networks	**NASA CALIPSO**	**ESA Aeolus**
1930s	1960	1963	1960-1990s	2000s	**2006**	**2018**

Overview

- Atmospheric Lidar Theory
- History of Lidar for Atmospheric Study
- **Recent Developments**

Georgia Tech Research Institute

Commercialization of Lidar

- Elastic backscatter lidar →
  - Droplet Measurement Technologies Micro Pulse Lidar
  - Ceilometers from Vaisala, Campbell Scientific
- Doppler wind lidar →
  - Vaisala WindCube
  - Halo Photonics Streamline Series
- DIAL →
  - Vaisala DA10 water vapor DIAL

Campbell Scientific SkyVue Pro

Droplet MPL

Vaisala WindCube

Vaisala DA10

Earth Cloud, Aerosol and Radiation Explorer (EarthCARE)

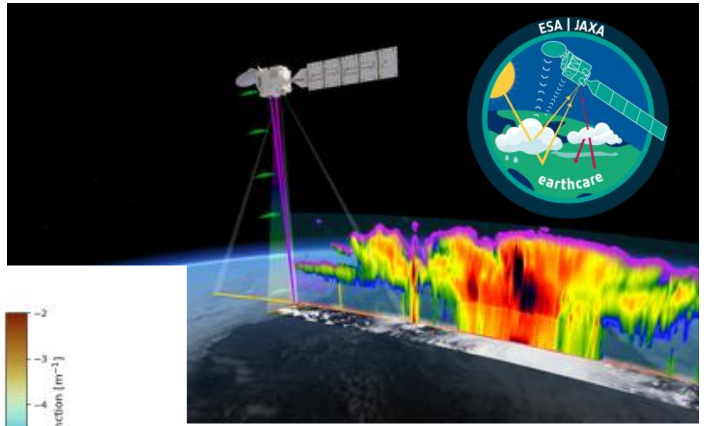

- ESA/JAXA mission to better understand Earth's thermal and solar radiation balance
- Expected launch date: May 2024
- Atmospheric lidar (ATLID)
  - HSRL
  - Depolarization lidar
  - For cloud-top, thin-cloud profiling, aerosol profiling
- Also includes:
  - Cloud profiling radar → penetrate clouds
  - Multispectral imager → wide-scene images
  - Radiometer → reflected & outgoing radiation

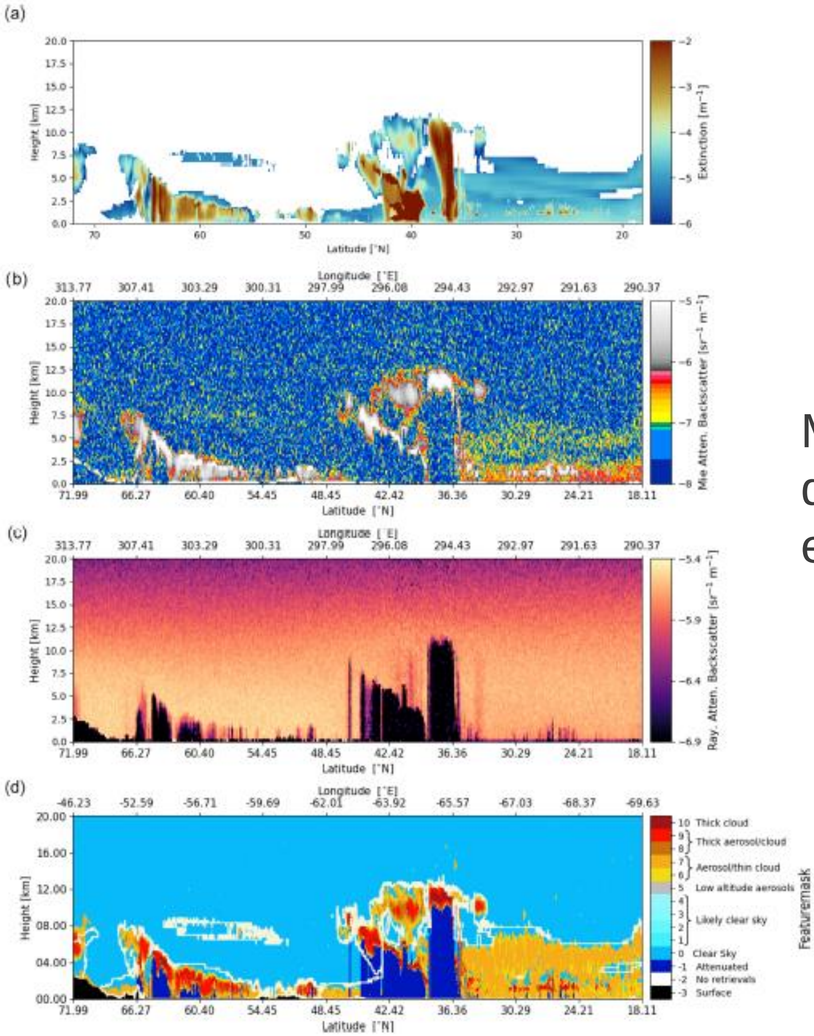

Figure 8. Halifax scene; panel **(a)** shows the input model extinction field, panel **(b)** shows the forward-modeled Mie co-polar signals, and panel **(c)** shows the forward-modeled co-polar Rayleigh attenuated-backscatter signals. Panel **(d)** depicts the retrieved FeatureMask for this scene with the $\alpha = 10^{-6}\ \mathrm{m}^{-1}$ model truth extinction contours on top in beige.

Modeled example data from Zadelhoff et al., 2023

Conclusions

- Light scattering interactions with molecules and particles have been employed as a method of atmospheric measurement for more than 90 years, with laser transmitters used in modern technology

- Many different types of atmospheric lidar enable atmospheric studies of:
  - Temperature & composition → Rayleigh, Raman, & Resonance Fluorescence lidar
  - Dynamics → Doppler wind lidar
  - Aerosols & air quality → elastic backscatter, Raman, & HSRL
  - Trace gases → DIAL & Raman lidar

- Recent advancements have brought atmospheric lidar technology to the commercial sector and new lidar systems continue to be deployed on major satellite programs

References

- Brown, E. A., Kim, H., Carr, D., Meraz, N., Craney, T., Patel, P., ... & Tuell, G. (2019, May). Seahawk lidar. In Laser Radar Technology and Applications XXIV (Vol. 11005, pp. 23-35). SPIE.
- Collis, R. T. H., & Russell, P. B. (2005). Lidar measurement of particles and gases by elastic backscattering and differential absorption. Laser monitoring of the atmosphere, 71-151.
- Cooney, J. (1972). Measurement of atmospheric temperature profiles by Raman backscatter. Journal of Applied Meteorology and Climatology, 11(1), 108-112.
- Dinoev, T., Simeonov, V., Arshinov, Y., Bobrovnikov, S., Ristori, P., Calpini, B., ... & van den Bergh, H. (2013). Raman lidar for meteorological observations, RALMO–Part 1: Instrument description. Atmospheric Measurement Techniques, 6(5), 1329-1346.
- Eloranta, E. E. (2005). High spectral resolution lidar. In Lidar: Range-resolved optical remote sensing of the atmosphere (pp. 143-163). New York, NY: Springer New York.
- Fernald, F. G., Herman, B. M., & Reagan, J. A. (1972). Determination of aerosol height distributions by lidar. Journal of Applied Meteorology and Climatology, 11(3), 482-489.
- Fernald, F. G. (1984). Analysis of atmospheric lidar observations: some comments. Applied optics, 23(5), 652-653.
- Fiocco, G., & Smullin, L. D. (1963). Detection of scattering layers in the upper atmosphere (60–140 km) by optical radar. Nature, 199(4900), 1275-1276.
- Gimmestad, G. G. (2005). Differential-absorption lidar for ozone and industrial emissions. In Lidar: Range-Resolved Optical Remote Sensing of the Atmosphere (pp. 187-212). New York, NY: Springer New York.
- Gross, S., Freudenthaler, V., Wiegner, M., Gasteiger, J., Geiss, A., & Schnell, F. (2012). Dual-wavelength linear depolarization ratio of volcanic aerosols: Lidar measurements of the Eyjafjallajökull plume over Maisach, Germany. Atmospheric Environment, 48, 85-96.
- Hair, J. W., Hostetler, C. A., Cook, A. L., Harper, D. B., Ferrare, R. A., Mack, T. L., ... & Hovis, F. E. (2008). Airborne high spectral resolution lidar for profiling aerosol optical properties. Applied optics, 47(36), 6734-6752.
- Hauchecorne, A., & Chanin, M. L. (1980). Density and temperature profiles obtained by lidar between 35 and 70 km. Geophysical Research Letters, 7(8), 565-568.
- Hulburt, E. O. (1937). Observations of a searchlight beam to an altitude of 28 kilometers. JOSA, 27(11), 377-382.
- Johnson, E. A., Meyer, R. C., Hopkins, R. E., & Mock, W. H. (1939). The measurement of light scattered by the upper atmosphere from a search-light beam. JOSA, 29(12), 512-517.
- Klett, J. D. (1981). Stable analytical inversion solution for processing lidar returns. Applied optics, 20(2), 211-220.
- Leblanc, T., Brewer, M. A., Wang, P. S., Granados-Muñoz, M. J., Strawbridge, K. B., Travis, M., ... & Newchurch, M. J. (2018). Validation of the TOLNet lidars: The southern California ozone observation project (scoop). Atmospheric measurement techniques, 11(11), 6137-6162.
- Leonard, D. A., & Caputo, B. (1974). A single-ended atmospheric transmissometer. Optical Engineering, 13(1), 10-14.
- Maiman, T. H. (1960). Stimulated optical radiation in ruby.
- Omar, A. H., Winker, D. M., Vaughan, M. A., Hu, Y., Trepte, C. R., Ferrare, R. A., ... & Liu, Z. (2009). The CALIPSO automated aerosol classification and lidar ratio selection algorithm. Journal of Atmospheric and Oceanic Technology, 26(10), 1994-2014.
- Pappalardo, G., Amodeo, A., Apituley, A., Comeron, A., Freudenthaler, V., Linné, H., ... & Wiegner, M. (2014). EARLINET: towards an advanced sustainable European aerosol lidar network. Atmospheric Measurement Techniques, 7(8), 2389-2409.
- Shipley, S. T., Tracy, D. H., Eloranta, E. W., Trauger, J. T., Sroga, J. T., Roesler, F. L., & Weinman, J. A. (1983). High spectral resolution lidar to measure optical scattering properties of atmospheric aerosols. 1: Theory and instrumentation. Applied optics, 22(23), 3716-3724.
- Stillwell, R. A., Spuler, S. M., Hayman, M., Repasky, K. S., & Bunn, C. E. (2020). Demonstration of a combined differential absorption and high spectral resolution lidar for profiling atmospheric temperature. Optics express, 28(1), 71-93.
- Moller, A., & Fernandez-Diaz, J. C. (2019). Airborne lidar for archaeology in Central and South America. Lidar Magazine, 1.
- Synge, E. H. (1930). XCI. A method of investigating the higher atmosphere. The London, Edinburgh, and Dublin Philosophical Magazine and Journal of Science, 9(60), 1014-1020.
- Welton, E. J., Campbell, J. R., Spinhirne, J. D., & Scott III, V. S. (2001, February). Global monitoring of clouds and aerosols using a network of micropulse lidar systems. In Lidar remote sensing for industry and environment monitoring (Vol. 4153, pp. 151-158). SPIE.
- Welton, E. J., Stewart, S. A., Lewis, J. R., Belcher, L. R., Campbell, J. R., & Lolli, S. (2018). Status of the NASA Micro Pulse Lidar Network (MPLNET): overview of the network and future plans, new version 3 data products, and the polarized MPL. In EPJ Web of Conferences (Vol. 176, p. 09003). EDP Sciences.
- Winker, D. M., Hostetler, C. A., Vaughan, M. A., & Omar, A. H. (2006). CALIOP algorithm theoretical basis document, part 1: CALIOP instrument, and algorithms overview. Release, 2, 29.
- Yuan, T., Solomon, S. C., She, C. Y., Krueger, D. A., & Liu, H. L. (2019). The long-term trends of nocturnal mesopause temperature and altitude revealed by Na lidar observations between 1990 and 2018 at midlatitude. Journal of Geophysical Research: Atmospheres, 124(12), 5970-5980.
- van Zadelhoff, G. J., Donovan, D. P., & Wang, P. (2023). Detection of aerosol and cloud features for the EarthCARE atmospheric lidar (ATLID): the ATLID FeatureMask (A-FM) product. Atmospheric Measurement Techniques, 16(15), 3631-3651.

Questions?

With acknowledgments to Irina Sokolik, Nathan Meraz, Jack Wood, Ryan James, and Dave Roberts

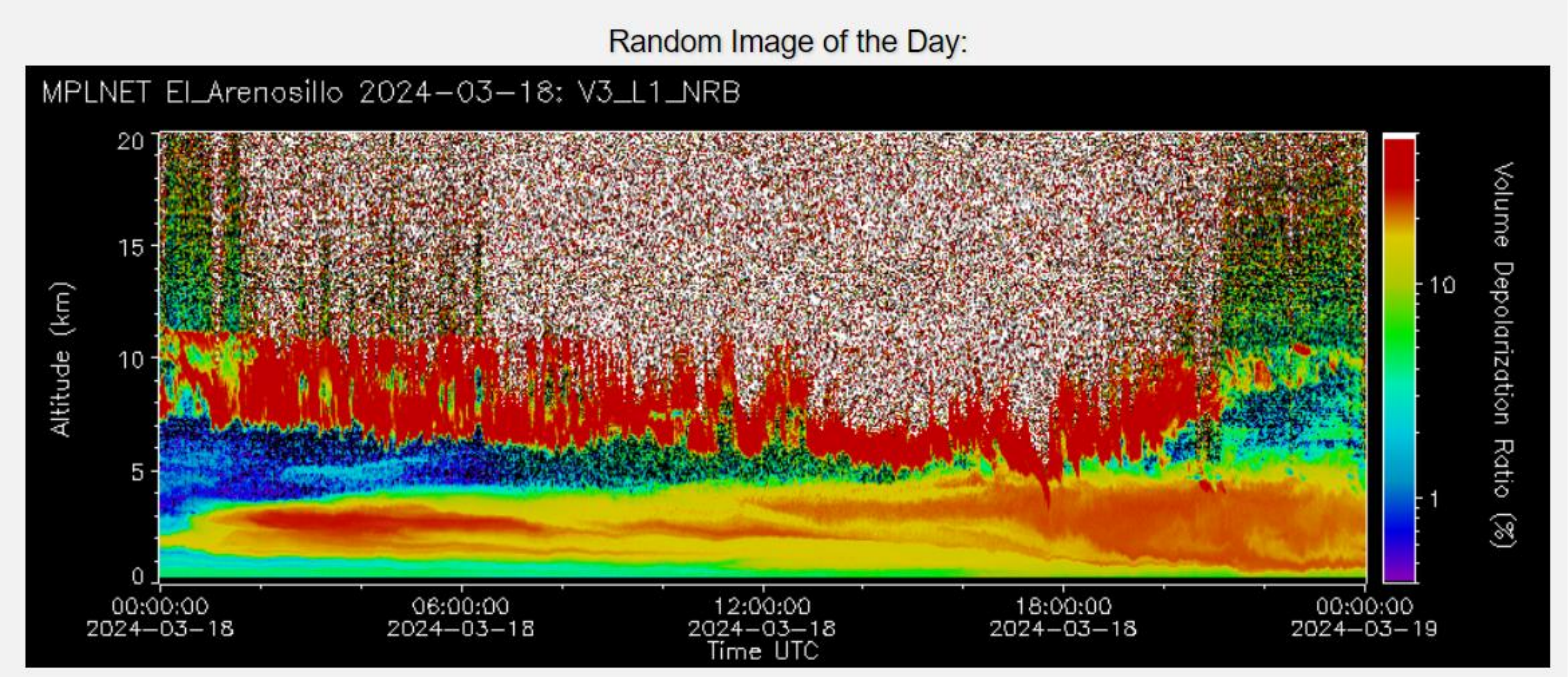

MPLNET Data from March 18, 2024 @ El Arenosillo in Doñana National Park, Spain:
https://mplnet.gsfc.nasa.gov/data-policy